Available online at www.sciencedirect.com
SCIENCE DIRECT®
International Journal of Heat and Fluid Flow 26 (2005) 513–525
International Journal of HEAT AND FLUID FLOW
www.elsevier.com/locate/ijhff

Onset of convection and finite amplitude flow due to Soret effect within a horizontal sparsely packed porous enclosure heated from below

M. Bourich [a], M. Hasnaoui [a,*], A. Amahmid [a], M. Mamou [b]

[a] Faculty of Sciences Semlalia, Department of Physics, LMFE, BP 2390 Marrakech, Morocco
[b] National Research Council Canada, Ottawa, Ont., Canada K1A 0R6

Received 19 December 2003; received in revised form 10 December 2004; accepted 14 January 2005
Available online 3 March 2005

Abstract

The Soret effect on thermal natural convection within a horizontal porous enclosure heated uniformly from below by a constant heat flux is studied analytically and numerically using the Brinkman–extended Darcy model along with the Boussinesq approximation. The governing parameters of the problem are the Darcy–Rayleigh number, R_T, the Lewis number, Le, the separation parameter, φ, the Darcy number, Da, and the aspect ratio of the enclosure, A_r. In the limit of a shallow enclosure, an analytical closed form solution is obtained on the basis of a parallel flow approximation. A numerical study is also conducted to validate the results of the analytical predictions. The thresholds for the onset of stationary and finite amplitude convection are determined explicitly as function of Le, φ and Da. The obtained results show that in the φ–Le plane there exists three regions that correspond to different parallel flow regimes, namely the subcritical and supercritical flows. The separation parameter has a strong effect on the threshold of instabilities and on the characteristics of heat and mass transfer. The threshold for Hopf bifurcation is obtained on the basis of the linear stability analysis. The wavenumber and the oscillation frequency at the onset of instabilities are null for an infinite extent layer.

Keywords: Heat and mass transfer; Analytical and numerical study; Thermosolutal convection; Soret effect

1. Introduction

Recent interest in the study of thermal and solutal diffusion in fluid and porous media has been motivated by its diverse engineering applications such as in hydrology, petrology, material processing technology where melting and solidification of binary alloys are involved, and geophysics. Convection in horizontal systems of multi-component fluids subject to vertical gradient of temperature has received considerable interest during the two last decades. Typically, the system considered is a horizontal layer of a binary fluid in a uniform gravitational field. Such system, becomes unstable when heated from below and generates solute concentration gradient known as the Soret effect, which is characterized by the separation parameter, φ, proportional to the thermodiffusion coefficient D'. When φ is positive, the heavier component migrates towards the cold upper wall, and to the bottom heated wall when φ is negative. In the former case, instabilities, that set in at the threshold of stationary convection, grow in a monotonic manner. In the latter case, subcritical and overstable convection may exist below the threshold of stationary convection. Beyond, the onset of overstability (Hopf bifurcation), instabilities grow in an oscillatory manner. The final state could be stationary or oscillatory leading

* Corresponding author. Tel.: +212 44 43 4649; fax: +212 44 43 7410.
E-mail address: hasnaoui@ucam.ac.ma (M. Hasnaoui).

0142-727X/$ - see front matter © 2005 Elsevier Inc. All rights reserved.
doi:10.1016/j.ijheatfluidflow.2005.01.001

Nomenclature

A_r	aspect ratio of the porous matrix, L'/H' (dimensionless)
D	mass diffusivity (m^2/s)
D'	thermodiffusion coefficient (m^2/K s)
Da	Darcy number, $\mu_{eK}/\mu H'^2$ (dimensionless)
g	gravitational acceleration (m/s^2)
H'	height of the porous cavity (m)
K	permeability of the porous medium (m^2)
L'	length of the porous cavity (m)
Le	Lewis number, α/D (dimensionless)
Nu	Nusselt number, Eq. (9) (dimensionless)
q'	constant heat flux per unit area
R_T	thermal Darcy–Rayleigh number, $g\beta_T K\Delta T' H'/(\alpha v)$ (dimensionless)
R_{TC}	critical thermal Rayleigh number (dimensionless)
S	dimensionless solute concentration, $S = S'/\Delta S'$
Sh	Sherwood number, Eq. (9) (dimensionless)
$\Delta S'$	characteristic difference of solute concentration, $\Delta S' = -\Delta T' S'_0 D'/D$ (kg/m^3)
t	dimensionless time, $t'\alpha/\sigma L'^2$
T	dimensionless temperature, $T = (T' - T'_0)/\Delta T'$
T'_0	reference temperature (K)
$\Delta T'$	characteristic difference of temperature, $\Delta T' = q'H'/\lambda$ (K)
(u, v)	dimensionless velocities in (x, y) directions $(u'H'/\alpha, v'H'/\alpha)$
(x, y)	dimensionless coordinates $(x'/H', y'/H')$

Greeks

α	thermal diffusivity of the porous medium, $\lambda/(\rho\ C)_f$ (m^2/s)
β_S	solutal expansion coefficient (m^3/kg)
β_T	thermal expansion coefficient (K^{-1})
ε	normalized porosity, ε'/σ (dimensionless)
φ	separation parameter, $\varphi = \beta_S \Delta S'/(\beta_T \Delta T')$ (dimensionless)
λ	thermal conductivity of the saturated porous medium (W/m^2 K)
v	kinematic viscosity of the fluid (m^2/s)
μ	dynamic viscosity of the fluid (kg/s m^2)
μ_e	effective viscosity (kg/s m^2)
ρ	density of the fluid mixture (kg/m^3)
$(\rho C)_F$	heat capacity of the fluid (W/K)
$(\rho C)_S$	heat capacity of the saturated porous medium (W/K)
σ	heat capacity ratio, $(\rho C)_F/(\rho C)_S$ (dimensionless)
ψ	dimensionless stream function, ψ'/α
ζ	dimensionless vorticity, $\zeta' H'^2/\alpha$

Subscripts

C	critical value
max	maximum value

Superscripts

$'$	dimensional variable
Hopf	Hopf bifurcation
sub	subcritical
sup	supercritical

to stationary or traveling waves. Below the threshold of overstabilities, the system becomes unstable only to finite amplitude perturbations.

Earlier, Hurle and Jakeman (1971) studied experimentally and theoretically thermosolutal convection driven by the Soret effect within a horizontal layer filled with a water–methanol mixture and heated from below. Above the threshold of Hopf bifurcation, the flow initially oscillated and then bifurcated towards a finite amplitude flow. The theoretical prediction for the threshold of instability was consistent with the experimental results. The hydrodynamic stability in non-reactive binary fluids within a large horizontal aspect ratio layer heated from below or from above was investigated by Gutkowicz-Krusin et al. (1979a,b). The thresholds of stationary and oscillatory convection were predicted using the variational approach. The wavenumber and the oscillation frequency were obtained as functions of the governing parameters. The effect of different thermal boundary conditions was considered by Knobloch and Moore (1988) in a horizontal cavity filled with 3He–4He fluid mixtures. Non-slip boundary conditions and a zero outward mass flux were considered to simulate experimental boundary conditions. On the basis of the linear stability analysis, the thresholds for the onset of stationary and oscillatory convection were predicted for different flow mixtures and thermal boundary conditions, and the codimension-2 point was determined. Results concerning the influence of Soret-induced solutal buoyancy forces on natural convection of an initially uniform concentration fluid contained in an enclosure heated from the side have been reported by Bergman and Srinivasan (1989). The authors found that, for real fluids, Soret contributions to the hydrodynamic mechanisms, which were responsible for variations in heat transfer rates, were apparently limited to water-based binary solutions near the density inversion temperature. Chavepeyer et al. (1999) investigated numerically the influence of the Soret effect on Marangoni convection in rectangular enclosures heated from the side. The sur-

face flow was found to inhibit the Soret separation down to the percent order.

In saturated porous enclosures, Karcher and Müller (1994) studied the Bénard convection of a binary liquid in a porous medium. The authors found that the mixture displayed negative Soret effects and showed a non-linear temperature dependence of the binary fluid density. For the case of a two-dimensional convection, traveling waves and steady-state solutions were observed. Thermogravitational separation in a binary mixture contained within a differentially heated enclosure with the presence of obstacles was studied numerically by Chavepeyer and Platten (1998). The Soret coefficient was found to be independent of the presence of the obstacles when considering a pure thermal diffusive regime. The onset of thermogravitational diffusion in a porous medium saturated with a binary mixture subjected to Soret effect was investigated numerically by Marcoux et al. (1998). The case of opposing and equal solutal and thermal buoyancy forces was considered. The thresholds of instability were obtained for various aspect ratios. Their numerical results showed different flow structures and the existence of time-periodic oscillatory solutions. Benano-Melly et al. (2001) considered thermal diffusion induced by a horizontal thermal gradient in a binary mixture within a porous medium. Their study showed that, depending on the Soret coefficient value, multiple convective flow patterns can develop when solutal and thermal buoyancy forces are opposing each other. Using the Galerkin technique, the onset of thermosolutal convection in a fluid saturated horizontal porous layer, subject to a gravity gradient was studied by Alex and Patil (2001). The authors showed that the Soret parameter affects the convective pattern only when its magnitude is large enough, in both the presence and the absence of gravity field variations. The onset of Soret-driven convection in a shallow porous enclosure saturated with a binary fluid has been discussed recently by Sovran et al. (2001). Heating from below or from the top, the criteria for the onset of motion via a stationary, Hopf bifurcation and oscillatory convection were derived. More recently, Bahloul et al. (2003) studied numerically and analytically, natural convection in a horizontal Darcy porous layer filled by a binary fluid. Both cases of double-diffusive and Soret-induced convections were considered. The critical Rayleigh numbers for the onset of supercritical, overstable and oscillatory convections were determined in terms of the governing parameters.

In the present study, the Brinkman–extented Darcy model is considered for a sparsely packed porous medium, which is an extention of a previous preliminary work using Darcy model by Bourich et al. (2002). The influence of the Soret effect on the natural convective flows induced within a shallow enclosure heated from below by a constant flux of heat were studied. Assuming parallel flow in the central region of the enclosure, an analytical solution is presented to predict explicitely the thresholds of stationary and finite amplitude flows, and heat and mass transfer characteristics. A numerical solution of the full governing equations is also presented for finite aspect ratio of the enclosure to validate the analytical results. The results showed a good agreement between the analytical predictions and the numerical simulations when the aspect ratio of the enclosure is large enough. A linear stability analysis is also carried out to investigate the onset of overstabilities.

2. Mathematical formulation

The system under study is a two-dimensional horizontal porous layer of width L' and height H'. The origin of the coordinate system (x' is the horizontal axis and y' is the vertical axis opposing gravity) is taken at the center of the cavity. All boundaries of the porous matrix are assumed rigid and impermeable. The short vertical walls of the porous layer are adiabatic while a uniform flux of heat, q', is imposed on its long horizontal walls. The porous matrix is assumed isotropic and homogeneous, and the Brinkman–extended Darcy law is adopted. The diluted binary solution that saturates the porous matrix, with an initial uniform concentration, is modeled as a Boussinesq incompressible fluid whose density varies according to

$$\rho = \rho_0[1 - \beta_T(T' - T'_0) - \beta_S(S' - S'_0)] \tag{1}$$

where ρ_0 is the binary fluid density at temperature $T' = T'_0$ and concentration $S' = S'_0$. The subscript 0 refers to conditions at the origin of the coordinates system.

Using the vorticity-stream function formulation, the dimensionless governing equations are written as follows:

$$\zeta = Da\nabla^2\zeta + R_T\left(\frac{\partial T}{\partial x} + \varphi\frac{\partial S}{\partial x}\right) \tag{2}$$

$$\nabla^2 T = \frac{\partial T}{\partial t} + u\frac{\partial T}{\partial x} + v\frac{\partial T}{\partial y} \tag{3}$$

$$\frac{1}{Le}(\nabla^2 S - \nabla^2 T) = \varepsilon\frac{\partial S}{\partial t} + u\frac{\partial S}{\partial x} + v\frac{\partial S}{\partial y} \tag{4}$$

$$\nabla^2\psi = -\zeta \tag{5}$$

$$u = \frac{\partial\psi}{\partial y}, \quad v = -\frac{\partial\psi}{\partial x} \tag{6}$$

The hydrodynamic, thermal and concentration boundary conditions are

$$x = \pm A_r/2, \quad \psi = \frac{\partial\psi}{\partial x} = 0, \quad \frac{\partial T}{\partial x} = \frac{\partial S}{\partial x} = 0 \tag{7a}$$

$$y = \pm 1/2, \quad \psi = \frac{\partial \psi}{\partial y} = 0, \quad \frac{\partial T}{\partial y} = \frac{\partial S}{\partial y} = -1 \tag{7b}$$

Eqs. (2)–(7) indicate that the present problem is governed by five dimensionless parameters. Namely, the thermal Darcy–Rayleigh number, R_T, the Lewis number, Le, the separation parameter, φ, the Darcy number, Da, and the aspect ratio of the enclosure, A_r. They are defined as

$$R_T = \frac{g\beta_T k \Delta T' H'}{\alpha \nu}, \quad Le = \frac{\alpha}{D}, \quad \varphi = \frac{\beta_S \Delta s'}{\beta_T \Delta T'},$$
$$Da = \frac{\mu_e K}{\mu H'^2}, \quad A_r = \frac{L'}{H'} \tag{8}$$

The Nusselt and Sherwood numbers are respectively defined by

$$Nu = \frac{1}{T(0,-1/2) - T(0,1/2)} \quad \text{and}$$
$$Sh = \frac{1}{S(0,-1/2) - S(0,1/2)} \tag{9}$$

Note that, in Eq. (9), Sh represents the solute concentration difference across the layer induced by the thermodiffusion phenomenon; the net mass flux across the layer being zero.

3. Numerical method

The solution of the full governing equations is obtained numerically using a finite difference scheme. The vorticity-stream function formulation is used and the vorticity equation (Eq. (2)) is written in its transient form to accelerate the convergence. The solution is obtained iteratively using the alternating direction implicit method (ADI). The values of the vorticity are calculated using the Wood's relation (Roache, 1982). The temperature and concentration equations (Eqs. (3) and (4)) are also solved using the ADI procedure. Nodal values of the stream function were obtained, from Eq. (5) via a point successive-over-relaxation method (PSOR). For situations where large aspect ratios are considered, a non-uniform grid was used to capture flow details near the boundaries.

The results reported in this paper were performed with 121×61 grid for $A_r = 4$ and 201×81 for $A_r \geqslant 8$. More details concerning the numerical method and the relaxation technique are given in the reference by Amahmid et al. (1999a).

4. Analytical approach

In the limit of a shallow enclosure ($A_r \gg 1$), it has been demonstrated in the past by several authors (see, for instance, Cormack et al. (1975) and Amahmid et al. (1999a)) that the present problem can be significantly simplified and analytically solved using the parallel flow approximation. Therefore, in the central part of the cavity, this approximation leads to the following simplifications:

$$\psi(x,y) = \psi(y), \quad T(x,y) = C_T x + \theta_T(y) \quad \text{and}$$
$$S(x,y) = C_S x + \theta_S(y) \tag{10}$$

where C_T and C_S are respectively unknown temperature and concentration gradients in the x-direction.

Using the approximation given in Eq. (10), the steady simplified form of the full governing equations (2)–(4) is obtained as :

$$Da \frac{d^4\psi}{dy^4} - \frac{d^2\psi}{dy^2} + E_r = 0 \tag{11}$$

$$\frac{d^2\theta_T}{dy^2} = C_T \frac{d\psi}{dy} \tag{12}$$

$$\frac{d^2\theta_S}{dy^2} = (Le\, C_S + C_T) \frac{d\psi}{dy} \tag{13}$$

where

$$E_r = -R_T(C_T + \varphi C_S) \tag{14}$$

The boundary conditions in the y-direction are now given by

$$y = \pm \frac{1}{2}, \quad \psi = \frac{d\psi}{dy} = 0, \quad \frac{d\theta_T}{dy} = \frac{d\theta_S}{dy} = -1 \tag{15}$$

By solving Eqs. (11)–(13) and taking into account the boundary conditions (15), a closed form solution is obtained as follows:

$$\psi(y) = \frac{E_r}{2}\left[\frac{\cosh(\Omega/2) - \cosh(\Omega y)}{\Omega \sinh(\Omega/2)} + y^2 - \frac{1}{4}\right] \tag{16}$$

$$u(y) = \frac{E_r}{2}\left[-\frac{\sinh(\Omega y)}{\sinh(\Omega/2)} + 2y\right] \tag{17}$$

$$T(x,y) = C_T x - y - \frac{C_T E_r}{2}\left[\frac{\sinh(\Omega y) - \Omega \cosh(\Omega/2) y}{\Omega^2 \sinh(\Omega/2)} - \frac{y^3}{3} + \frac{y}{4}\right] \tag{18}$$

$$S(x,y) = C_S x - y - \frac{E_r(Le\, C_S + C_T)}{2} \times \left[\frac{\sinh(\Omega y) - \Omega \cosh(\Omega/2) y}{\Omega^2 \sinh(\Omega/2)} - \frac{y^3}{3} + \frac{y}{4}\right] \tag{19}$$

where $\Omega = \frac{1}{\sqrt{Da}}$.

According to Eq. (17), the velocity cannot be zero in the range $0 < y < 1/2$. This implies that only monocellular flows are possible. It is noted that with the parallel

flow approximation, the thermal and solutal boundary conditions cannot be satisfied in the x-direction. Instead, the expressions for C_T and C_S were determined by considering that the heat and mass transfer rates across any transversal section of the porous layer are zero (Trevisan and Bejan, 1986). This yields

$$C_T = \frac{-AE_r}{1+BE_r^2} \quad \text{and}$$
$$C_S = \frac{-AE_r(1+Le)}{(1+BE_r^2)(1+BLe^2E_r^2)} \tag{20}$$

Upon combining Eqs. (14) and (20), it is found that

$$E_r = \pm\left[\frac{-b \pm \sqrt{b^2-4Le^2c}}{2BLe^2}\right]^{\frac{1}{2}} \tag{21}$$

where $b = (1+Le^2) - ALe^2R_T$ and $c = 1 - AR_T[1 + (1+Le)\varphi]$. The positive constants A and B depend on the Darcy number as

$$A = \frac{1}{\Omega^2} + \frac{1}{12} - \frac{2}{f},$$
$$B = \frac{6}{f^2} + \frac{1}{\Omega^2 f} - \frac{1}{3f} - \frac{1}{8\Omega^2} - \frac{2}{\Omega^4} + \frac{1}{120} \tag{22}$$

where $f = 4\Omega\tanh(\Omega/2)$.

Then, the Nusselt and Sherwood numbers are given by

$$Nu = \frac{1+BE_r^2}{1+(B-A^2)E_r^2} \quad \text{and} \quad Sh = \frac{1}{\frac{B-A^2}{B} + \frac{A^2(1-BLeE_r^2)}{B(1+BE_r^2)(1+BLe^2E_r^2)}} \tag{23}$$

In Eq. (21), E_r is negative for clockwise flows and positive for counterclockwise flows. In both situations, the Nusselt and Sherwood numbers remain the same. For convenience, only the solution corresponding to positive E_r is considered. The solution with positive sign within the square root in Eq. (21) will be denoted by E_{r^+} and the solution with the negative sign by E_{r^-}. These two solutions exist only when the following conditions are satisfied:

$$-b \pm \sqrt{b^2-4Le^2c} > 0 \quad \text{and} \quad b^2 - 4Le^2c > 0 \tag{24}$$

According to (24), the existence of three regions in the φ–Le plane, that correspond to different parallel flow solutions, is obtained. In the first region, stationary convection also called supercritical convection (the convective flow bifurcates from the rest state through a zero amplitude convection) is possible. The domain that delineates this region is defined by

$$\varphi \geqslant \varphi_1(Le) = \frac{-1}{(1+Le)(1+Le^2)} \tag{25}$$

The critical Rayleigh number, R_{TC}^{sup}, above which the convective flow is possible is given by

$$R_{TC}^{sup} = \frac{R^{sup}}{1+(1+Le)\varphi} \tag{26}$$

where $R^{sup} = 1/A$ and A is given in Eq. (22). The second region indicates that both subcritical and stationary convection solutions are possible. This region is delimited by

$$\frac{-1}{1+Le} < \varphi < \frac{-1}{(1+Le)(1+Le^2)} \tag{27}$$

The critical Rayleigh number, R_{TC}^{sub}, for the onset of subcritical flows (the convective flow occurs through a finite amplitude convection) is given by

$$R_{TC}^{sub} = \frac{Le+1}{Le^2}\left[Le - 1 - 2\varphi + 2\sqrt{-\varphi(Le-1-\varphi)}\right]R^{sup} \tag{28}$$

Finally, in the third region, only subcritical flows are possible. This region is defined by

$$\varphi \leqslant \varphi_2(Le) = \frac{-1}{1+Le} \tag{29}$$

The subcritical Rayleigh number is given by the same expression as that for region 2 (Eq. (28)). At this stage, according to the parallel flow approximation, it should be recalled that the rest state solution becomes unstable to finite amplitude perturbations for $R_T > R_{TC}^{sub}$ and unstable to infinitesimal perturbations when $R_T > R_{TC}^{sup}$.

For this type of problem, as discussed recently by Sovran et al. (2001), a Hopf bifurcation can occur within the range $R_{TC}^{sub} < R_T < R_{TC}^{sup}$. In the present study, for an infinite porous layer, the linear stability analysis based on the Galerkin method, as reported by Mamou et al. (1998) and Bahloul et al. (2003), is used to determine the threshold for which the Hopf bifurcation occurs. Assuming a small perturbation amplitude, the solution is decomposed into a rest state solution, and the following perturbation profile:

$$\left.\begin{aligned} \Psi &= 0 + \psi_0 e^{pt+ikx}F(y) \\ T &= -y + \theta_0 e^{pt+ikx}G(y) \\ S &= -y + \phi_0 e^{pt+ikx}G(y) \end{aligned}\right\} \tag{30}$$

where F and G are y-dependent functions describing the perturbation profile, k is the wavenumber and p is the growth rate. The parameters ψ_0, θ_0 and ϕ_0 are the perturbation amplitudes.

The linear governing equations, after neglecting the second order terms, are obtained as follows:

$$\begin{cases} \psi_0\left(\frac{d^2F}{dy^2} - K^2F\right) = Da\,\psi_0\left(\frac{d^4F}{dy^4} - 2K^2\frac{d^2F}{dy^2} + K^4F\right) \\ \qquad\qquad -ikGR_T(\theta_0 + \varphi\phi_0) \\ p\theta_0G + ik\psi_0F = \theta_0\left(\frac{d^2G}{dy^2} - K^2G\right) \\ \varepsilon Le\,p\phi_0G + ik\psi_0 LeF = (\theta_0 - \phi_0)\left(\frac{d^2G}{dy^2} - K^2G\right) \end{cases} \tag{31}$$

The corresponding boundary conditions are:

$$F = \frac{\partial F}{\partial y} = \frac{\partial G}{\partial y} = 0 \tag{32}$$

Using the perturbation profiles F and G as the weighted functions in the Galerkin method, the integrated equations lead to the dispersion relationship as described in Mamou et al. (1998) and Bahloul et al. (2003). The onset of Hopf bifurcation is obtained when the growth rate p becomes a pure imaginary number $p = 0 + i\omega$, where ω is the circular frequency. Solving the dispersion equation for the Rayleigh number, the critical Rayleigh number for the onset of Hopf bifurcation is obtained as follows:

$$R_{TC}^{Hopf} = \frac{(\varepsilon Le + 1)}{Le(\varepsilon + \varphi)} R^{sup} \tag{33}$$

where R^{sup} is the critical Rayleigh number for the onset of pure thermal convection. The constant R^{sup} is found to depend only on the Darcy number and it reaches its minimum value when $k \to 0$. For this situation, the Hopf bifurcation occurs at zero wavenumber and zero oscillation frequency for an infinite horizontal layer. However, the frequency is finite for a finite aspect ratio enclosure but it decreases by increasing A_r. More details concerning this point are given in the following sections.

From Eq. (33), it is clear that the occurrence of the oscillatory flow depends not only on Le and φ (as it is the case for R_{TC}^{sub} and R_{TC}^{sup}) but also on ε; it is therefore obvious that when $\varphi \leqslant -\varepsilon$, this regime does not exist.

5. Results and discussion

The main objective of the numerical simulations conducted in this part of the paper is to validate the results of the analytical predictions based on the parallel flow approximation. The influence of φ, Le and Da on the critical Rayleigh numbers for the onset of convective parallel flow and Hopf bifurcation is discussed first. Then the effect of the governing parameters on the flow intensity (ψ_0) and the heat and mass transfer characteristics (Nu and Sh), in the different regions previously defined, is discussed.

5.1. Effect of φ, Le and Da on the critical Rayleigh numbers

The influence of the separation parameter φon the critical Rayleigh numbers, R_{TC}^{sub}, R_{TC}^{sup} and R_{TC}^{Hopf}, is illustrated in Fig. 1 for $Da = 0.01$, $Le = 10$ and $\varepsilon = 0.95$. The curve corresponding to R_{TC}^{sub} and R_{TC}^{sup} shows a monotonous decrease (slow decrease in the case of R_{TC}^{sub}) with φ when this parameter is increased from -1 to $+1$. Note also that for $\varphi = 0$, the supercritical Rayleigh number, $R_{TC}^{sup}(\varphi = 0) = 1/A$, becomes independent of Le, since the flow depends on the temperature field

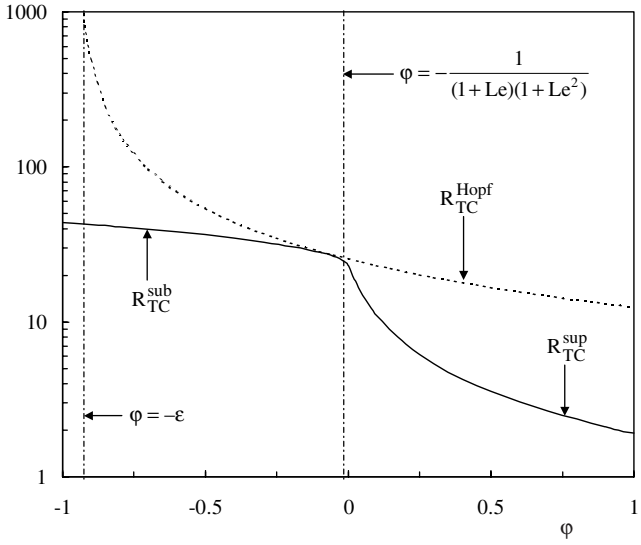

Fig. 1. Effect of φ on the critical Rayleigh numbers for $Da = 0.01$, $\varepsilon = 0.95$ and $Le = 10$.

solely. As shown in Fig. 1, for $\varphi > 0$, R_{TC}^{sup} is lower than the critical value corresponding to the pure thermal convection. In fact, for $\varphi > 0$, the thermodiffusion phenomenon has a destabilizing effect which causes an early appearance of convection. However, for $\varphi < 0$, the solute transfer has a stabilizing effect and as a matter of fact the onset of convective flows is retarded ($R_{TC}^{sub} > R_{TC}^{sup}(\varphi = 0)$).The evolution of R_{TC}^{Hopf} with φ is characterized by a monotonous decrease from $+\infty$ to 12.43 as φ increases from $-\varepsilon = -0.95$ to $+1$.

The effect of the Lewis number on the critical Rayleigh numbers is presented in Fig. 2 for $Da = 0.01$ and $\varepsilon = 0.95$. The thresholds of convection, R_{TC}^{sup}, R_{TC}^{sub} and R_{TC}^{Hopf} are obtained, respectively, for $\varphi = 0.5$, -1

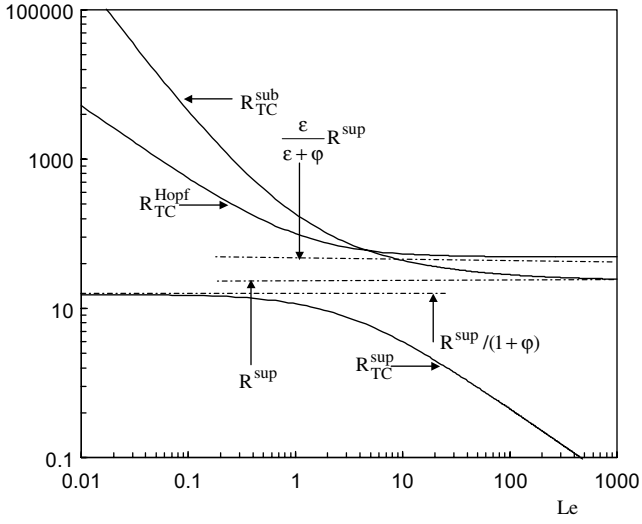

Fig. 2. Effect of Le on the critical Rayleigh numbers for $Da = 0.01$ and $\varepsilon = 0.95$.

and −0.5. The choice of these values of φ is imposed by the different ranges of this parameter for which the various convective modes (supercritical, subcritical and Hopf bifurcations) are possible. As shown in Fig. 2, the supercritical Rayleigh number, R_{TC}^{sup}, decreases monotonically from its asymptotic limit $R^{sup}/(1+\varphi)$, obtained for small Le, to $R^{sup}/(Le\,\varphi)$ for large Le. Consequently, the supercritical Rayleigh number tends towards zero when Le becomes high enough. Concerning the evolution of R_{TC}^{sub} with Le, it is characterized by a continuous decrease towards its asymptotic limit R^{sup} at large Le. For small values of the latter parameter, the threshold of subcritical convection can be approximated by the expression $R_{TC}^{sub} \cong 2R^{sup}[\sqrt{\varphi(\varphi+1)}-\varphi)-1]/Le^2$; this explains why $R_{TC}^{sub} \to +\infty$ at small Le. The last critical Rayleigh number, R_{TC}^{Hopf}, corresponding to the onset of Hopf bifurcation shows similar evolution with Le as that described for R_{TC}^{sub} with $R_{TC}^{Hopf} = \varepsilon R^{sup}/(\varepsilon+\varphi)$ as asymptotic limit at large Le. For small values of Le, the threshold of Hopf bifurcation can be approximated by $R_{TC}^{Hopf} \cong R^{sup}/(\varphi+\varepsilon)Le$ which shows why large values of R_{TC}^{Hopf} are needed to promote oscillatory convection for this case.

The evolution of R^{sup} with Da is illustrated in Fig. 3 where it is seen that this parameter increases with Da and this increase becomes linear with an important slope for $Da > 0.1$ (fluid medium). In addition, the variation of R^{sup} with Da is characterized by an asymptotic behavior for small Da and the value of the asymptote is 12. The latter value is well known in the literature for R^{sup} in the case of Darcy medium.

5.2. Effect of Rayleigh number

The Rayleigh number, R_T, is a measure of the thermal driving force. It could be varied by changing the heat flux intensity or by considering various working fluids or different porous media with different permeabilities.

The effect of R_T on the flow characteristics and heat and mass transfer is now examined for different regions. Fig. 4(a)–(c) show respectively the evolutions of the flow intensity, $\psi_0 = \psi(0,0)$, the Nusselt number, Nu, and the Sherwood number, Sh, with R_T for $Da = 0.01$ and different combinations of (Le, φ). The parallel flow solutions presented here are those corresponding to $E_r = E_{r^+}$ and $E_r = E_{r^-}$. It is noted that the solutions corresponding

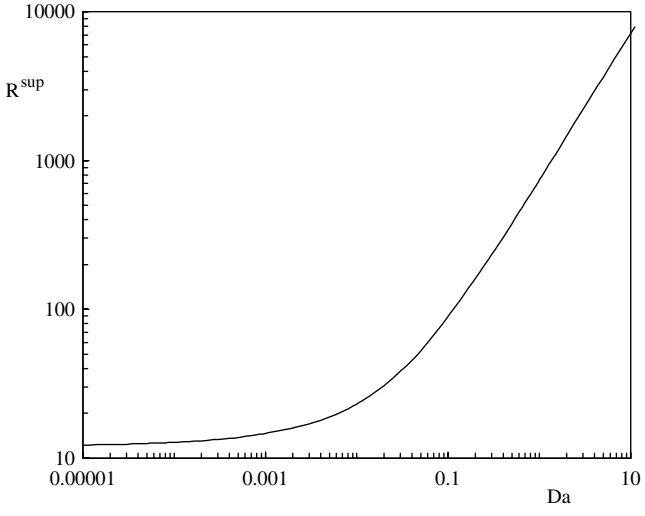

Fig. 3. Effect of Da on R^{sup}.

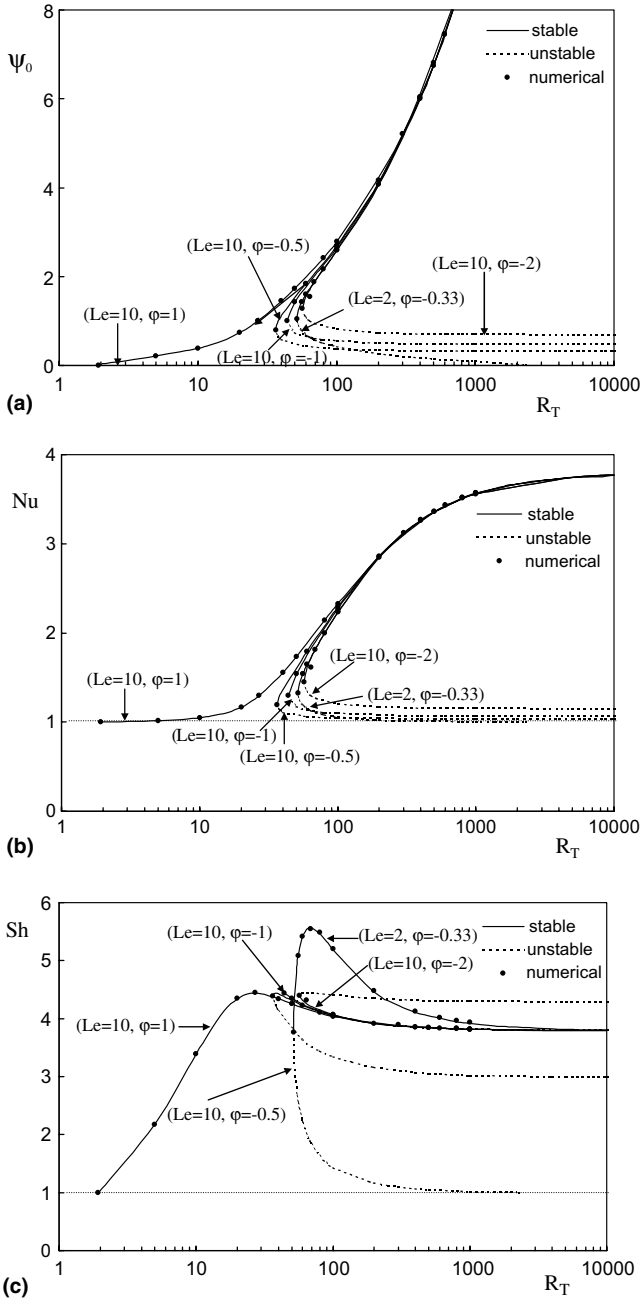

Fig. 4. Effect of R_T on (a) ψ_0, (b) Nu and (c) Sh for $Da = 0.01$ in different regimes.

to $E_r = \pm E_{r^-}$ were not obtained numerically despite the multiple trial and errors using different initial conditions. Hence, the solution $E_r = \pm E_{r^-}$ is believed to be unstable. In the following discussion, the solutions $E_r = \pm E_{r^-}$ and $E_r = \pm E_{r^-}$ will be termed as "stable" and "unstable" branches, respectively. The analytical solutions for ψ_0, Nu and Sh corresponding to stable branches are seen to be in excellent agreement with the numerical ones obtained by solving the full governing equations.

For $(Le, \varphi) = (10, 1)$, which corresponds to region 1, only the stable branch is existing. The supercritical convection starts from the rest state at $R_{TC}^{sup} = 1.923$ and Nu and Sh tend respectively to the same asymptotic limit $Nu = Sh = 3.791$ for large values of R_T (Fig. 4(b) and (c)), while ψ_0 increases monotonically with this parameter (Fig. 4(a)). In fact, at sufficiently large values of R_T, the analytical expression of E_{r^+} can be approximated by

$$E_{r^+} \cong \pm\sqrt{\frac{AR_T}{B}} \tag{34}$$

which means that E_{r^+} and ψ_0 increase as $R_T^{1/2}$. In addition, the constants C_T and C_S tend towards zero since they vary as $R_T^{-1/2}$ and $R_T^{-3/2}$, respectively. For such condition (high R_T), the quantities $C_T E_r$ and $(Le\, C_S + C_T)E_r$ reduce to

$$C_T E_r = (Le\, C_S + C_T)E_r = -\frac{A}{B} \tag{35}$$

As a consequence, the temperature and the concentration profiles become identical at large R_T. This explains why both Nu and Sh (Eq. (23)) lead to the same asymptotic value given by $Nu = Sh = \frac{B}{B - A^2}$. A similar asymptotic behavior has already been reported and discussed in detail by Amahmid et al. (1999b) in the case of a horizontal Brinkman porous layer submitted to constant fluxes of heat and mass in the absence of the Soret effect. In addition, before reaching the asymptotic value, Sh is seen to pass through a maximum value $Sh_{max} \cong 4.442$ at $R_T \cong 26.94$.

The region 2 is illustrated in Fig. 4(a)–(c) by the combination $(Le, \varphi) = (2, -0.33)$. The fluid motion starts through finite amplitude convection at $R_{TC}^{sub} \cong 51.67$. The stable branch of Sh corresponding to region 2 reaches a maximum value $Sh_{max} \cong 5.569$ at $R_T \cong 68.45$. For regions 1 and 2, the analytical expression of the maximum R_T at which Sh exhibits maximum value is given by

$$R_{T\,max} = \frac{R^{sup}(1 + Le)(\sqrt{Le} + 1)^2}{Le\sqrt{Le}(1 + \sqrt{Le} + \varphi)} \tag{36}$$

Eq. (36) shows that $R_{T\,max}$ is depending on the parameters Le, Da and φ. For the unstable branch the quantities ψ_0, Nu and Sh are observed to decrease by increasing R_T and this branch vanishes for $R_T \geqslant R_{TC}^{sup} \cong 2307.93$. Before its disappearance, the unstable solution joins the pure diffusive regime solution. The limiting expressions of E_r, ψ_0, Nu and Sh corresponding to the stable branch, in region 2, are similar to those obtained in region 1 when R_T is high enough.

Fig. 5(a) displays the bifurcation diagram in terms of the flow intensity as a function of the Rayleigh number for $Da = 0.01$, $\varepsilon = 0.5$ and $(Le, \varphi) = (2, -0.33)$. According to the parallel flow approximation and the linear stability analysis, the different critical Rayleigh numbers that delineate different flow regimes for this case are $R_{TC}^{sub} = 51.7$, $R_{TC}^{Hopf} = 135.8$ and $R_{TC}^{sup} = 2307.9$. These values are obtained for an infinite extent layer. For finite aspect ratio enclosure, i.e. $A_r = 4$ for example, it was found that, $R_{TC}^{Hopf} = 142$. To compare with the finite amplitude flows, a numerical solution of the full governing equations is examined near the threshold of overstabilities. As predicted by the linear stability analysis, beyond the onset of instabilities, the flow amplitude grows in an oscillatory manner. The value $R_T = 145$ is selected for illustration. As shown in Fig. 5(b), the flow amplitude exhibits exponential growth with oscillation. For this situation, the convective flow circulation is

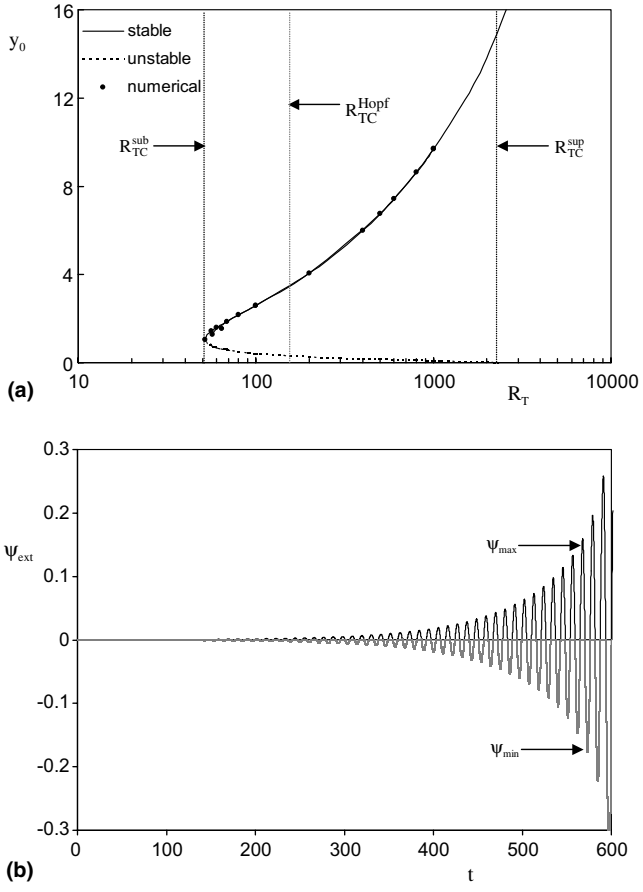

Fig. 5. Bifurcation diagram (a) and oscillatory flows near the onset of Hopf bifurcation (b) for $Da = 0.01$, $\varepsilon = 0.5$, $(Le, \varphi) = (2, -0.33)$ and $A_r = 4$.

changing from clockwise to counterclockwise direction or vice versa. This is in agreement with the linear stability prediction. However, as the time goes, it was observed that when the non-linear effects become significant, the oscillatory flows bifurcate towards steady monocellular or multi-cellular flows (results not presented).

At the early stage of convection, the oscillation frequency is observed to decrease drastically with the increase of the aspect ratio A_r. For $A_r = 4$, 8 and 12 the oscillation period is obtained respectively as $\tau = 10.7$, 40.4 and 96.0. For relatively large aspect ratio enclosure, a mathematical correlation is derived as $\tau = 0.66A_r^2$. The latter demonstrates clearly that the oscillation frequency vanishes ($f_r = 2\pi/\tau$) for an infinite layer, which is in agreement with the linear stability analysis prediction.

As can be derived from Eqs. (26) and (33), the codimension-2 point at which overstabilities and stationary convection coexist, is obtained as follows:

$$R_T = \frac{\varepsilon Le(Le+1)+1}{\varepsilon Le(Le+1)-1}R^{sup} \quad \text{and} \quad \varphi = \frac{-1}{\varepsilon Le(Le+1)+1} \tag{37}$$

The above expressions demonstrate that overstabilities set in only for negative separation ratio. Eq. (33) shows that, when $\varphi \leqslant -\varepsilon$, overstabilities do not exist and the system becomes unconditionally stable. However, the parallel flow approximation, which is regarded as a non-linear stability analysis, showed that there exists a threshold for convection above which the system becomes unstable to finite amplitude perturbations. Also it is worth to mention that, according to the numerical solution (not given here), Bénard convection (muticellular flows) within the porous layer is possible and becomes the preferred mode far from the criticality.

Finally, in region 3, represented by the combinations $(Le, \varphi) = (10, -0.5)$, $(10, -2)$ and $(10, -1)$ in Fig. 4(a)–(c), the stable and unstable branches exist for any value of $R_T \geqslant R_{TC}^{sub}$. In this region, the quantities Nu and Sh that correspond to the stable branch exhibit also asymptotic behaviors with R_T, which are similar to those observed for the stable branches in regions 1 and 2. For the unstable branch and high values of R_T, the expression of E_{r^-} can be approximated as

$$E_{r^-} \cong \pm\sqrt{-[1+(1+Le)\varphi]/B}/Le \tag{38}$$

Then, ψ_0, Nu and Sh have an asymptotic evolution with R_T and the asymptotic values depend on Le, Da and φ. Note that the three values of (Le, φ) were presented in Fig. 4(a)–(c) in region 3 because they lead to different behaviors in terms of Sherwood number. In fact, depending on the range of φ, the Sherwood number corresponding to the stable branch (Fig. 4(c)) may be lower than, higher than or identical to the one corresponding to the unstable branch for $-1 < \varphi \leqslant -\frac{1}{1+Le}$, $\varphi < -1$ and $\varphi = -1$, respectively. In addition, for the stable branch, Sh passes through a maximum at $R_T = R_{T\max}$ (Eq. (36)) and $R_T = R_{TC}^{sup}$ (Eq. (26)) for $-1 < \varphi \leqslant -\frac{1}{1+Le}$ and $\varphi \leqslant -1$, respectively.

By comparing the asymptotic behaviors observed in the three different regions, the velocity increases as $R_T^{1/2}$ (for large R_T) for the stable branches, whereas the temperature and the concentration profiles (and thereby Nu and Sh) become identical and independent of R_T, Le, φ and the considered region. The asymptotic values of Nu and Sh for these branches are such that $Nu = Sh = B/(B - A^2)$. For the unstable branches in region 3, the velocity, temperature and concentration profiles become independent of R_T but remain dependent on Da, Le and φ, for large R_T.

The evolution of Sh with R_T can be explained by examining each term of the solute equation (Eq. (4)). According to the parallel flow approximation, the solute equation indicates that the mass transfer is ruled by the competition between the convective mass transfer, the solutal diffusion and the Soret effect. Eq. (4) reduces to

$$\frac{1}{Le}\nabla^2 S - \frac{1}{Le}\nabla^2 T = u\frac{\partial S}{\partial x} \tag{39}$$

The integration of Eq. (39) from $y = -1/2$ to y, leads to

$$\frac{\partial S}{\partial y} - \frac{\partial T}{\partial y} = Le\,C_S\int_{-1/2}^{y} u(y)\,dy = Le\,C_S\psi(y) \tag{40}$$

Integrating Eq. (40) from $y = -1/2$ to $y = 1/2$, yields

$$\frac{1}{Sh} = \frac{1}{Nu} - \frac{A^2 Le(1+Le)E_r^2}{(1+BE_r^2)(1+BLe^2E_r^2)} \tag{41}$$

Eq. (41) implies that, independently of R_T, Le, Da and φ, $Sh \geqslant Nu$ (i.e. $\Delta S' \leqslant \Delta T'$). The maximum of Sh is reached when the convective effect is important. By increasing R_T, the convective mass transfer in the horizontal direction, represented by the second term on the right-hand side of Eq. (41), increases from zero in region 1 and from positive values in regions 2 and 3 towards a maximum value obtained at $R_{TC\,max} = \frac{1+Le}{ALe(1+\varphi)}$. Above this threshold, the convective mass transfer decreases towards zero when R_T becomes high enough. Consequently, the solute equation represents now only a balance between solutal diffusion and Soret effect which explains the same asymptotic limit observed for Nu and Sh. However, for intermediate values of R_T in the vicinity of $R_{TC\,max}$, the convective mass transfer term is important, which explains the maximum value of Sh. According to the above results, we conclude that the Soret effect can change significantly the concentration distribution inside the cavity. Note that, the maximum is not observed for Sh in the absence of thermal diffusion effect (Amahmid et al., 1999b).

5.3. Effect of Lewis number

The Lewis number describes the relative importance of the thermal diffusivity with respect to the solute diffusivity. This parameter depends on the nature of the working fluid and its mean temperature. The Lewis number could be also varied by changing the mean solute concentration within the porous layer.

Some interesting asymptotic behaviors of the parallel flow, observed at small and large values of Le, are discussed. The asymptotic results, corresponding to $Le \to 0$, depend on the region considered. In region 1 ($\varphi > -1$), the unstable branch is absent and the constant E_{r^+}, corresponding to the stable branch, can be approximated by

$$E_{r^+} \cong \pm\sqrt{A[R_T(1+\varphi)-1]/B} \tag{42}$$

This implies that, when $Le \to 0$ the flow intensity and Nu and Sh depend on R_T, Da and φ. In addition, the constants C_T and C_S have the same limit leading to identical profiles for the temperature and concentration. These profiles, can be deduced by introducing

$$\begin{aligned} E_r C_T &= E_r(C_T + Le\, C_S) \\ &= [1 - AR_T(1+\varphi)]/[ABR_T(1+\varphi)] \end{aligned} \tag{43}$$

in Eqs. (18) and (19). As a result, Nu and Sh exhibit the same limits. In region 3 ($\varphi \leqslant -1$), the asymptotic limits depend on the considered branch. The parameter E_{r^+} corresponding to the stable branch at small Le and $R_T \geqslant R_{TC}^{sub}(\varphi = -1)$ reduces to

$$E_{r^+} = \pm\sqrt{\frac{AR_T}{B}} \tag{44}$$

As $R_{TC}^{sub} \to +\infty$ when $Le \to 0$, then $|E_{r^+}| \to +\infty$, $|\psi_0| \to +\infty$ and the asymptotic values of Nu and Sh tend towards $B/(B - A^2)$. In addition, when $Le \to 0$, the limiting expression of the parameter E_{r^-} is given by

$$E_{r^-} \cong \pm\sqrt{-(1+\varphi)/B}/Le \tag{45}$$

Consequently, the limiting values of ψ_0, Nu and Sh are identical to those corresponding to the stable branch discussed above for $\varphi \leqslant 1$.

At large values of Le, the asymptotic limits depend on the sign of φ. For the case of opposing thermal and solutal buoyancy forces ($\varphi < 0$), both stable and unstable branches exist. The constant E_{r^-} tends towards its pure thermal convection value ($\varphi = 0$) given by

$$E_{r^+} \cong \pm\sqrt{(AR_T - 1)/B} \tag{46}$$

which becomes independent of φ at large Le, but it remains dependent on R_T and Da. Therefore, the flow and the heat transfer rate are those of pure thermal convection showing negligible effect of the Soret effect. The concentration profile depends on R_T and Da and its expression is obtained by introducing the relation $E_r Le\, C_S = -1/BR_T$ in Eq. (19). The asymptotic limit of Sh corresponding to the stable branch, which depends only on Da, is given by $Sh = B/(B - A^2)$. For $Le \to +\infty$, the parameter E_{r^-} can be approximated by

$$E_{r^-} \cong \pm\sqrt{\frac{AR_T\varphi}{B(1-AR_T)Le}} \tag{47}$$

Thus, Eq. (47) shows that E_{r^-} varies as $Le^{-1/2}$. This means that the fluid flow and the heat transfer rates are identical to those corresponding to the pure diffusive regime ($\psi_0 = 0, Nu = 1$) while the concentration profiles and the mass transfer are identical to those of the stable branch. For $\varphi > 0$, the solute is destabilizing, the unstable branch does not exist and the limiting expression of E_{r^+} depends on R_T solely when $Le \to +\infty$. The expressions of E_r are given by Eqs. (46) and (47) for $R_T > R_{TC}^{sup}(\varphi = 0) = 1/A$ and $R_T < R_{TC}^{sup}(\varphi = 0) = 1/A$, respectively. For $R_T = R_{TC}^{sup}(\varphi = 0) = 1/A$, the limiting expression of E_r is given by:

$$E_r \cong \pm\sqrt{(\sqrt{\varphi/Le})/B} \tag{48}$$

This implies that, at large Le, the heat transfer rate and the flow intensity are identical to those corresponding to pure thermal convection and pure diffusive regime for $R_T > R_{TC}^{sup}(\varphi = 0)$ and $R_T \leqslant R_{TC}^{sup}(\varphi = 0)$, respectively. However, the concentration profile and the Sherwood number, obtained at large Le, are independent of R_T and they are identical to those obtained with $\varphi < 0$.

5.4. Effect of Darcy number

The Darcy number, Da, depends directly on the permeability of the porous material and the width of the layer. It is very small for well packed porous medium and relatively large for sparsely packed porous medium. For small value of Da, the viscous effects are confined within a thin layer near the boundaries.

The effect of Da on ψ_0, Nu and Sh is illustrated respectively in Fig. 6(a)–(c) for $R_T = 100$ and $(Le, \varphi) = (10, 0)$, $(1.5, -0.2)$ and $(10, -0.5)$. The combination values of (Le, φ) correspond respectively to regions 1, 2 and 3. It can be seen that the numerical results are in excellent agreement with the analytical ones corresponding to the stable branch. The quantities ψ_0, Nu and Sh decrease by increasing Da, for the stable branch. However, for the unstable branch, (when it exists), the effect of Da remains negligible in general. Note also that, for each region, the parallel flow solution vanishes when Da exceeds a critical value, Da_C. Fig. 6(a)–(c) show also that for $(Le, \varphi) = (10, 0)$, which corresponds to the case where the flow is induced by the thermal convection, $Da_C \cong 0.1153$ and the only possible solution is that of the stable branch which tends towards the rest state solution as Da approaches Da_C. For region 1, the

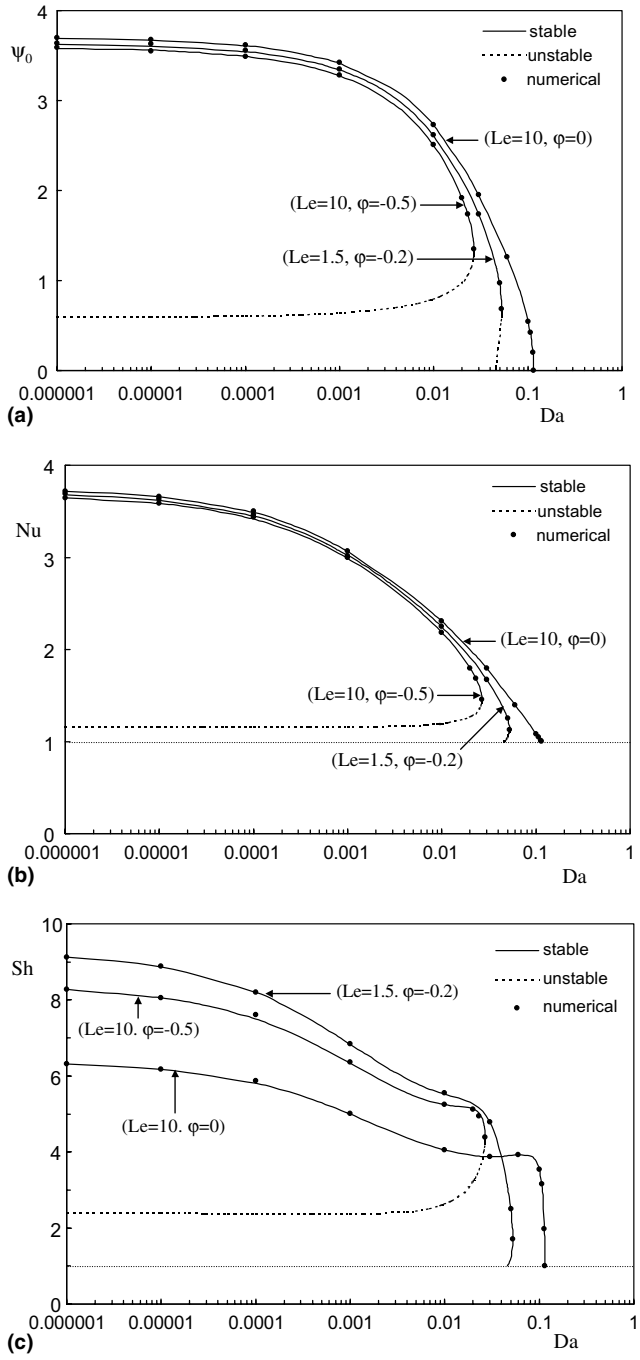

Fig. 6. Effect of Da on (a) ψ_0, (b) Nu and (c) Sh for $R_T = 100$ in different regimes.

critical value, Da_C, can be computed (for given R_T, Le and φ) by solving the following equation

$$A(Da_C) = \frac{1}{R_T[1 + \varphi(1 + Le)]} \tag{49}$$

For region 2, illustrated by $(Le, \varphi) = (10, -0.2)$ in Fig. 6(a)–(c), the stable branch exists for $0 \leqslant Da \leqslant Da_C = 0.0525$ while the unstable branch exists only for $0.0462 \leqslant Da \leqslant 0.0525$. In fact for this region, there exists a critical value of Da, below which the unstable branch disappears. Note that the convective solution corresponding to the unstable branch starts from the rest state at $Da = 0.0462$. For the case corresponding to $(Le, \varphi) = (10, -0.5)$, both stable and unstable branches exist for $0 < Da \leqslant Da_C = 0.02667$ and the convective solution bifurcates through finite amplitude convection when $Da = Da_C$. For regions 2 and 3, Da_C is obtained by solving the following expression

$$A(Da_C) = \frac{Le + 1}{R_T Le^2}[Le - 1 - 2\varphi + 2\sqrt{-\varphi(Le - 1 - \varphi)}] \tag{50}$$

5.5. Effect of the separation parameter φ

The separation ratio, φ, can be widely varied by changing the mean solute concentration or the mean temperature of the system.

The influence of the Soret effect on the flow intensity and heat and mass transfer rates is examined for given values of R_T, Le and Da. Fig. 7(a)–(c) illustrate the evolution of ψ_0, Nu and Sh with φ for $R_T = 100$, $Da = 0.01$ and $Le = 0.1$ and 10. The figures show an excellent agreement between the numerical and analytical results corresponding to the stable branch. For $Le = 0.1$, the stable branch, which is the only existing solution for this case, starts from the rest state in region 1, at $\varphi_{C_1} \cong -0.693$. This critical value of φ can be computed by the following expression

$$\varphi_{C_1} = \frac{1 - AR_T}{(1 + Le)AR_T} \tag{51}$$

which is valid only when $R_T \leqslant R_T^{sup}(\varphi_{C1})$. This means, in view of Eq. (26), that

$$R_T \leqslant \frac{1 + Le^2}{A\,Le^2} \tag{52}$$

The increase of ψ_0, Nu and Sh, which have different behaviors, starts from $\varphi = \varphi_{C_1}$. The increase of ψ_0 with φ is monotonous while that of Nu and Sh exhibits asymptotic behavior. At sufficient large values of φ, the limiting expression of E_{r^+} is given by

$$E_{r^+} \cong \left[\frac{\sqrt{AR_T(1 + Le)\varphi}}{B\,Le}\right]^{\frac{1}{2}} \tag{53}$$

which implies that E_{r^+} and ψ_0 increase as $\varphi^{\frac{1}{4}}$. Furthermore, the constants C_T and C_S tend towards zero since they vary as $\varphi^{-\frac{1}{4}}$ and $\varphi^{-\frac{3}{4}}$, respectively. The terms $C_T E_r$ and $(Le\,C_S + C_T)E_r$ reduce to

$$C_T E_r = (Le\,C_S + C_T)E_r = -\frac{A}{B} \tag{54}$$

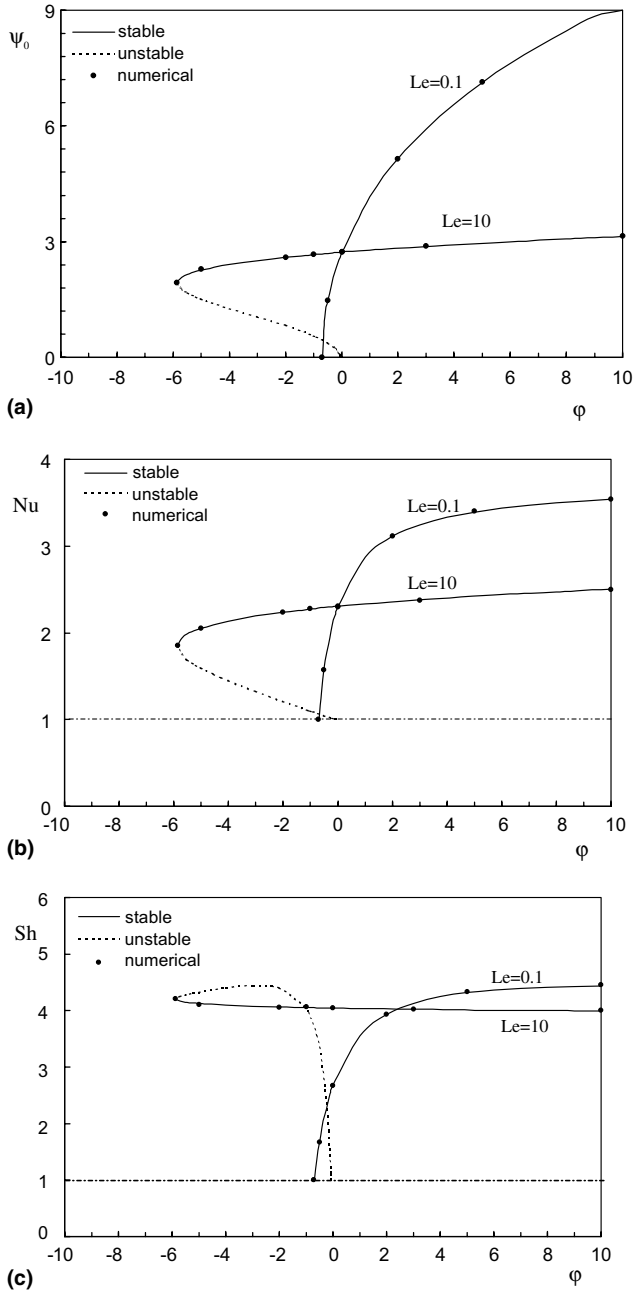

Fig. 7. Effect of φon (a) ψ_0, (b) Nu and (c) Sh for $R_T = 100$, $Da = 0.01$ and different Le.

implying that, for this limit, the temperature and concentration profiles become identical and, consequently, Nu and Sh have the same asymptotic value given by

$$Nu = Sh = \frac{B}{B - A^2} \tag{55}$$

Note that, although the asymptotic limit is the same for Nu and Sh, their evolution towards this asymptote presents some difference. These two parameters increase first significantly between φ_{C_1} and $\varphi \cong 5$ and then slightly when φ becomes large. However, the slow variation of Nu towards the asymptote is characterized by a monotonic increase while Sh passes through a maximum and decreases slightly towards the asymptotic value. For given values of R_T, Le and Da verifying the inequality of Eq. (52), the expression of φ_{max} at which the mass transfer rate reaches its maximum is given by

$$\varphi_{max} = \frac{(1+\sqrt{Le})[Le + \sqrt{Le}(1+Le) + Le^2(1 - AR_T)]}{A\,Le^2 R_T} \tag{56}$$

For $Le = 10$, both stable and unstable branches exist and the subcritical convection occurs at φ_{C_2} which can be computed by solving the following expression

$$\varphi - \sqrt{-\varphi(Le - 1 - \varphi)} = \frac{(1 - AR_T)Le^2 - 1}{2(Le + 1)} \tag{57}$$

The above expression is valid for $R_T \geqslant R_{TC}^{sub}(\varphi_{C_2})$, which corresponds to the following condition

$$R_T \geqslant \frac{(1+Le)^2}{A\,Le^2} \tag{58}$$

The critical value, φ_{C_2}, is -5.68 for the values of R_T and Le considered here. Qualitatively and quantitatively, the behaviors of ψ_0, Nu and Sh change significantly by increasing Le. Starting from φ_{C_2}, the variations of ψ_0 and Nu corresponding to the unstable branch are characterized by a continuous decrease towards the diffusive regime at $\varphi_{C_3} \cong 0.07$ (Eq. (51)). However, the evolution of Sh in the range $\varphi_{C_2} \leqslant \varphi \leqslant \varphi_{C_3}$ is different when compared to those of ψ_0 and Nu; it is characterized by a slight increase with φ followed by a drastic decrease towards the diffusive regime ($Sh = 1$). Concerning the stable branch, the monotonous increase of ψ_0 with φ is slower than that observed for $Le = 0.1$ and Nu and Sh have the same asymptotic limit. Their evolution towards the asymptotic value are characterized by a slight increase and decrease, respectively. Referring once again to Fig. 7(c), we note that, for $\varphi < -1$, Sh corresponding to the unstable branch is higher than that of the stable branch and the reverse is observed for $-1 < \varphi \leqslant \frac{1}{1+Le}$. However, at $\varphi = -1$, the value of Sh is the same for the two branches.

6. Conclusion

Soret driven thermosolutal convection in a horizontal porous layer subject to vertical constant flux of heat has been investigated analytically and numerically using the Brinkman–extended Darcy model. In the limit of a shallow enclosure, the analytical solution based on the parallel flow assumption is found to be in good agreement with the numerical results corresponding to the stable branches. The thresholds for the onset of stationary and finite amplitude flows are determined analytically as a function of Le, Da and φ. Similarly to the Darcy

medium, it is found that the φ–Le plane can be divided into three regions corresponding to different parallel flow regimes. In the first region, only the supercritical convection is possible. In the second region both supercritical and subcritical convection are possible. However, in the third region, only subcritical convection exists. The threshold of Hopf bifurcation is obtained using the linear stability analysis, the wavenumber and the oscillation frequency vanish at the onset of overstabilities for an infinite horizontal layer. It is found that the increase of the Darcy number delays the onset of the convective regimes. At large R_T and φ, the Nusselt and Sherwood numbers corresponding to the stable branches have the same asymptotic limit $Nu = Sh = B/(B - A^2)$ which depends only on Da. Depending on the value of φ, the Soret effect can affect considerably the characteristics of the fluid flow and the heat and mass transfer.

References

Alex, S.M., Patil, P.R., 2001. Effect of variable gravity field on Soret driven thermosolutal convection in a porous medium. Int. Commun. Heat Mass Transfer 28, 509–518.

Amahmid, A., Hasnaoui, M., Vasseur, P., 1999a. Etude analytique et numérique de la convection naturelle dans une couche poreuse de Brinkman doublement diffusive. Int. J. Heat Mass Transfer 42, 2991–3005.

Amahmid, A., Hasnaoui, M., Mamou, M., Vasseur, P., 1999b. Double-diffusive parallel flow induced in a horizontal Brinkman porous layer subjected to constant heat and mass fluxes: analytical and numerical studies. J. Heat Mass Transfer 35, 409–421.

Bahloul, A., Boutana, N., Vasseur, P., 2003. Double-diffusive and Soret-induced convection in a shallow horizontal porous layer. J. Fluid Mech. 491, 325–352.

Benano-Melly, L.P., Caltagirone, J.-P., Faissat, B., Montel, F., Costeseque, P., 2001. Modeling Soret coefficient measurement experiments in porous media considering thermal and solutal convection. Int. J. Heat Mass Transfer 44, 1285–1297.

Bergman, T.L., Srinivasan, R., 1989. Numerical simulation of Soret-induced double diffusion in an initially uniform concentration binary liquid. Int. J. Heat Mass Transfer 32, 679–687.

Bourich, M., Hasnaoui, M., Amahmid, A., Mamou, M., 2002. Soret driven thermosolutal convection in a shallow porous enclosure. Int. Commun. Heat Mass Transfer 29, 717–728.

Chavepeyer, G., Platten, J.K., 1998. Approche de la séparation thermogravitationnelle d'un liquide binaire en modèle aléatoire de milieux poreux par moyennes d'ensembles. Entropie 214, 27–30.

Chavepeyer, G., De Saedeleer, C., Pétré, G., 1999. Influence of the Soret effect on Marangoni convection in cells heated from the side. Entropie 218, 63–66.

Cormack, D.E., Leal, L.G., Imberger, J., 1975. Natural convection in a shallow cavity with differentially heated end walls. Part 1. Asymptotic theory. J. Fluid Mech. 65, 209–229.

Gutkowicz-Krusin, D., Collins, M.A., Ross, J., 1979a. Rayleigh–Bénard instability in nonreactive binary fluids. I. Results. Phys. Fluids 22, 1443–1450.

Gutkowicz-Krusin, D., Collins, M.A., Ross, J., 1979b. Rayleigh–Bénard instability in nonreactive binary fluids. II. Results. Phys. Fluids 22, 1451–1460.

Hurle, D.T., Jakeman, E., 1971. Soret-driven thermosolutal convection. J. Fluid Mech. 47, 667–687.

Karcher, C., Müller, U., 1994. Bénard convection in a binary mixture with a nonlinear density–temperature relation. Phys. Rev. E 49, 4031–4043.

Knobloch, E., Moore, D.R., 1988. Linear stability of experimental Soret convection. Phys. Rev. A 37, 860–870.

Mamou, M., Hasnaoui, M., Amahmid, A., Vasseur, P., 1998. Stability analysis of double-diffusive convection in a vertical Brinkman porous enclosure. Int. Commun. Heat Mass Transfer 25, 491–500.

Marcoux, M., Charrier-Mojtabi, M.C., Bergeon, A., 1998. Naissance de la thermogravitation dans un mélange binaire imprégnant un milieu poreux. Entropie 214, 31–36.

Roache, P., 1982. Computational fluid dynamics. Hermosa, Albuquerque, NM.

Sovran, O., Charrier-Mojtabi, M.C., Mojtabi, A., 2001. Naissance de la convection thermo-solutante en couche poreuse infinie avec effet Soret. Compte-Rendu de l'Académie des Sciences, Paris 329, 287–293.

Trevisan, O.V., Bejan, A., 1986. Mass and heat transfer by natural convection in a vertical slot filled with porous medium. Int. J. Heat Mass Transfer 29, 403–415.